

# 1 Why Did Ozone Concentrations Remain High During Shanghai's Static 2 Management? A Statistical and Radical Chemistry Perspective

3 Jian Zhu<sup>1</sup>, Shanshan Wang<sup>1,2</sup>, Chuanqi Gu<sup>1</sup>, Zhiwen Jiang<sup>1</sup>, Sanbao Zhang<sup>1</sup>, Ruibin Xue<sup>1</sup>, Yuhao Yan<sup>1</sup>, Bin  
4 Zhou<sup>1,2,3</sup>

5 <sup>1</sup>Shanghai Key Laboratory of Atmospheric Particle Pollution and Prevention (LAP<sup>3</sup>), Department of Environmental Science and  
6 Engineering, Fudan University, Shanghai, 200433, China.

7 <sup>2</sup>Institute of Eco-Chongming (IEC), Shanghai, 202162, China.

8 <sup>3</sup>Institute of Atmospheric Sciences, Fudan University, Shanghai, 200433, China.

9 *Correspondence to:* Bin Zhou ([binzhou@fudan.edu.cn](mailto:binzhou@fudan.edu.cn)) and Shanshan Wang ([shanshanwang@fudan.edu.cn](mailto:shanshanwang@fudan.edu.cn))

## 10 Abstract

11 During the period of April and May 2022, Shanghai implemented city-wide static management measures to control the spread of  
12 the Omicron variant. Compared to the lockdown in early 2020, the static management in 2022 occurred during the high-ozone  
13 season and lasted for a longer duration. It can be considered as a “large-scale field experiment” to study the response of ambient  
14 ozone levels to emission reductions. During this period, we conducted comprehensive observations at Fudan University  
15 Jiangwan Campus in the northeast corner of Shanghai. Similar experiments were also conducted during the same period in 2020  
16 and 2021. Despite the significant reduction of approximately 30% in VOCs and around 50% in NO<sub>2</sub> due to static management in  
17 2022, the average ozone level increased by nearly 23%, compared to 2020 and 2021. This suggests that the reduction in ozone  
18 precursors and other pollutants did not lead to a corresponding decrease in ozone concentrations as expected. Cluster analysis of  
19 diurnal patterns of ozone concentration revealed four distinct types of diurnal ozone variations. Cluster 3 and Cluster 4, with high  
20 ozone levels, experienced significant increases in their share during static management, ultimately leading to an overall increase  
21 in average ozone levels in 2022. According to the Observation-Based Model (OBM) simulation analysis, the average peak  
22 concentrations of OH, HO<sub>2</sub>, and RO<sub>2</sub> in 2022 were estimated to be  $5.1 \times 10^6$ ,  $4.7 \times 10^8$ , and  $2.6 \times 10^8$  molecules cm<sup>-3</sup>,  
23 respectively, representing an increase of about 30% compared to the levels in 2020 and 2021. Although HONO photolysis was  
24 the main contributor to the primary source of ROx radicals, the radical cycling process remained dominant for the overall  
25 production of ROx radicals. Due to a significant decrease in NO<sub>2</sub> concentration relative to VOCs, the average VOCs/NO<sub>2</sub> ratio  
26 increased from 1.6 in 2020 to 3.0 in 2022, which is also reflected in the radical cycling. The ratio of OH radical propagation  
27 (OH+VOCs) to termination (OH+NO<sub>2</sub>) was 2.37, higher than 1.18 in 2020 and 1.78 in 2021, indicating that the different  
28 reduction proportions of precursors led to a higher VOCs/NO<sub>2</sub> ratio, strengthening the radical cycling. The differential reduction  
29 in precursor VOCs and NO<sub>2</sub> levels due to static management is the underlying cause for the increase in ozone concentration in  
30 Shanghai.

## 31 1 Introduction

32 To curb the spread of Omicron variant in Shanghai, China, the local government decided to implement city-wide static  
33 management in early April 2022. The strict two-month lockdown severely impacted the economic activities and human life of  
34 this mega city. According to official statistics (<https://tjj.sh.gov.cn/sjfb/index.html>), in April and May 2022, Shanghai  
35 experienced a year-on-year decrease of 42% in its total industrial output value. Moreover, the total volume of transported goods  
36 decreased by 30% year-on-year, with road transport witnessing a significant drop of 64%. Additionally, the port cargo

37 throughput decreased by 31% year-on-year. The direct effect of such lockdown policies on air quality is a significant reduction in  
38 anthropogenic emissions, which can be considered as an ideal experiment on emissions control in a mega-city to explore the  
39 reduction potential and response of air quality . It makes sense to take advantage of this rare yet regrettable window to study the  
40 causes and management of air pollution, especially in countries like China that face complex air pollution issues.

41 Prior to this, China had implemented a series of nationwide lockdown measures against the occurrence and spread of the virus in  
42 early 2020. This reduction in human activity is expected to significantly reduce air pollutant emissions, as confirmed by lots of  
43 studies on lockdown in 2020 (Bao and Zhang, 2020; Huang et al., 2021; Li et al., 2021b; Liu et al., 2020; Tian et al., 2021; Wang  
44 et al., 2021; Zhang et al., 2022b). Reports on the impact of the lockdown on air quality most commonly focus on measuring  
45 nitrogen dioxide ( $\text{NO}_2$ ) and fine particulate matter ( $\text{PM}_{2.5}$ ) (Agarwal et al., 2020; Hua et al., 2021; Chu et al., 2021). According to  
46 satellite data, tropospheric nitrogen oxides ( $\text{NO}_x$ ) emissions have decreased by 30-60% compared to pre-lockdown levels (Feng  
47 et al., 2020; Ding et al., 2020; Venter et al., 2020). Similarly, surface  $\text{PM}_{2.5}$  levels in northern China have also decreased by  
48 approximately 35%. Meanwhile, the average  $\text{O}_3$  concentration has increased 1.5-2 times (Shi and Brasseur, 2020). In Wuhan, the  
49 urban area that implemented stringent measures to limit the spread of the coronavirus, concentrations of  $\text{PM}_{2.5}$ ,  $\text{NO}_2$ , and ozone  
50 also exhibited similar changes (Shi and Brasseur, 2020). Among these pollutants,  $\text{NO}_2$  from traffic sources has shown the most  
51 significant reduction, with traffic-related  $\text{NO}_2$  exhibiting the largest decrease (Rana et al., 2021; Wang et al., 2020). Huang et al.  
52 (2021) suggest that increase in  $\text{O}_3$  enhances atmospheric oxidation capacity, providing favorable conditions for the formation of  
53 secondary particulate matter. Due to the lockdown taking place during winter, which is a season of high particulate matter  
54 pollution in China, the reports on the impact of the lockdown on air quality have focused more on the changes in particulate  
55 matter. The lockdown in Shanghai in 2022 was implemented in April and May during the high-ozone ( $\text{O}_3$ ) season and lasted for  
56 a longer duration, providing an opportunity to study atmospheric pollution primarily caused by  $\text{O}_3$ .

57 Previous extensive research has demonstrated that the formation of  $\text{O}_3$  in response to its precursors is highly nonlinear, rather  
58 than linear, which presents a challenge in ozone control (Liu and Shi, 2021; Wang et al., 2017; Sillman, 1999). The COVID-19  
59 pandemic provided a costly experiment to validate this. During the static management period in Shanghai, despite a reduction in  
60 precursor emissions, the ozone levels increased compared to the previous year. The cause of this increase is attributed to an  
61 imbalance in the reduction ratio of nitrogen oxides ( $\text{NO}_x$ ) and volatile organic compounds (VOCs) rather than meteorological  
62 conditions, according to satellite observation results (Tan and Wang, 2022; Xue et al., 2022). In this current study, aim is to  
63 elucidate the reasons behind the increase in ozone levels in Shanghai through a comprehensive approach involving in-situ  
64 observations, mathematical analysis, and modeling. Benefiting from our conducted routine observational campaigns, we have  
65 obtained comprehensive observational data for both the static management period and corresponding historical periods. We  
66 initiated our analysis by comparing pollutant levels and diurnal variations during the static management period with those from  
67 historical reference periods. Subsequently, by clustering diurnal ozone profile patterns, we examined the reasons behind the  
68 elevated ozone levels from a statistical perspective. Furthermore, we discuss changes in radical chemistry compared to historical  
69 periods, shedding light on the increase in ozone concentrations from a photochemical process standpoint. It is worth mentioning  
70 that, based on previous researchs and our analysis, meteorological conditions are not considered to be the primary cause of the  
71 ozone increase during the static management period, even though we acknowledge that meteorological conditions are indeed  
72 important factors influencing ozone levels. The in-depth comparison of meteorological conditions is presented in Text S1 of the  
73 Supplement.

74 **2 Experimental Details and Methods**

75 **2.1 Location and Experimental Setup**

76 During the static management period in April and May of 2022, we conducted comprehensive observational experiments at  
77 Fudan University's Jiangwan Campus (31.34°N, 121.51°E), located in an urban area in northeastern Shanghai, China. Similar  
78 experiments were also conducted during the corresponding period in 2020 and 2021. The ambient concentrations of O<sub>3</sub>, NO<sub>2</sub>,  
79 SO<sub>2</sub>, HONO, and HCHO were measured using the Differential Optical Absorption Spectroscopy (DOAS) system located on the  
80 rooftop of the Environmental Science Building (Zhu et al., 2020; Guo et al., 2021; Zhu et al., 2022). Based on the given optical  
81 path length and integration time, the detection limits for O<sub>3</sub>, NO<sub>2</sub>, SO<sub>2</sub>, HONO, and HCHO were approximately 1.3 ppbv, 0.5  
82 ppbv, 0.1 ppbv, 0.1 ppbv, and 0.5 ppbv, respectively. The measurements were carried out with a time resolution of 5-6 minutes  
83 and detailed fitting configurations are available in Table S1. Non-methane volatile organic compounds (NMVOCs) were  
84 monitored in real-time using the TH-300B online monitoring instrument, which has been previously described in detail in  
85 previous reports (Gu et al., 2022; Zhu et al., 2020). The photolysis rate of NO<sub>2</sub> ( $j(\text{NO}_2)$ ) was measured using a filter radiometer  
86 (Meteorologieconsult GmbH, Germany). The meteorological parameters data such as pressure (P), temperature (TEMP), relative  
87 humidity (RH), wind speed (WS), wind direction (WD), and boundary layer height (BLH) are derived from the European Center  
88 for Medium-Range Weather Forecasts (ECMWF) atmospheric reanalysis product ERA5 and extracted from the nest where the  
89 measurement site is located. The PM<sub>2.5</sub> data was obtained from the Yangpu environment monitoring station (31.53°N, 121.25°E)  
90 near the measurement site.

91 **2.2 Observation-Based Model (OBM)**

92 The open-source zero-dimensional box model tool AtChem2 was used to simulate atmospheric chemical processes, which is  
93 specifically designed for use with the Master Chemical Mechanism (MCM) (Sommariva et al., 2020). The MCM, one of most  
94 widely used chemical mechanism for chemistry, is a near-explicit chemical mechanism which describes the degradation of  
95 methane and 142 nonmethane VOCs and over 17000 elementary reactions of 6700 primary, secondary and radical species  
96 (<http://mcm.york.ac.uk/>, last access: 16 January 2023) (Jenkin et al., 2003; Saunders et al., 2003). AtChem2 software and  
97 documentation can be found on <https://github.com/AtChem/> (last accessed on January 16, 2023).

98 In this study, the observed data of O<sub>3</sub>, NO<sub>2</sub>, SO<sub>2</sub>, HONO, HCHO, NMVOCs,  $j(\text{NO}_2)$ , P, T, RH, and BLH were used as inputs to  
99 constrain the model calculations. The photolysis rates of other molecules such as O<sub>3</sub>, HCHO, HONO, and OVOCS can be  
100 calculated in this model platform with the basic principle driven by the solar zenith angle and scaled by the measured  $J_{\text{NO}_2}$   
101 (Sommariva et al., 2020). The removal of all unconstrained and simulated species caused by the deposition is determined by a  
102 parameterization approach, and is determined by the accumulation of the deposition velocity of 0.01 m s<sup>-1</sup> within the boundary  
103 layer (Santiago et al., 2017). The sensitivity of simulation results to the deposition velocity has been studied in previous research,  
104 and the impact is limited (Zhu et al., 2020). The model outputs include the concentration of the hydroxyl radical (OH) and  
105 hydroperoxy radical (HO<sub>2</sub>), as well as the reaction rates at each step of the simulation process.

106 **2.3 Machine learning**

107 Two machine learning methods, k-means clustering and the stacking model, were utilized in this study. In order to investigate the  
108 reasons for the overall increase in ozone levels during the static management period from the perspective of its diurnal variation,  
109 the k-means clustering method was applied to cluster 24-hour time series of O<sub>3</sub> concentration (Zhang et al., 2004). Time-series  
110 clustering is a specific application of curve clustering, which is similar to trajectory clustering in the transport of air masses

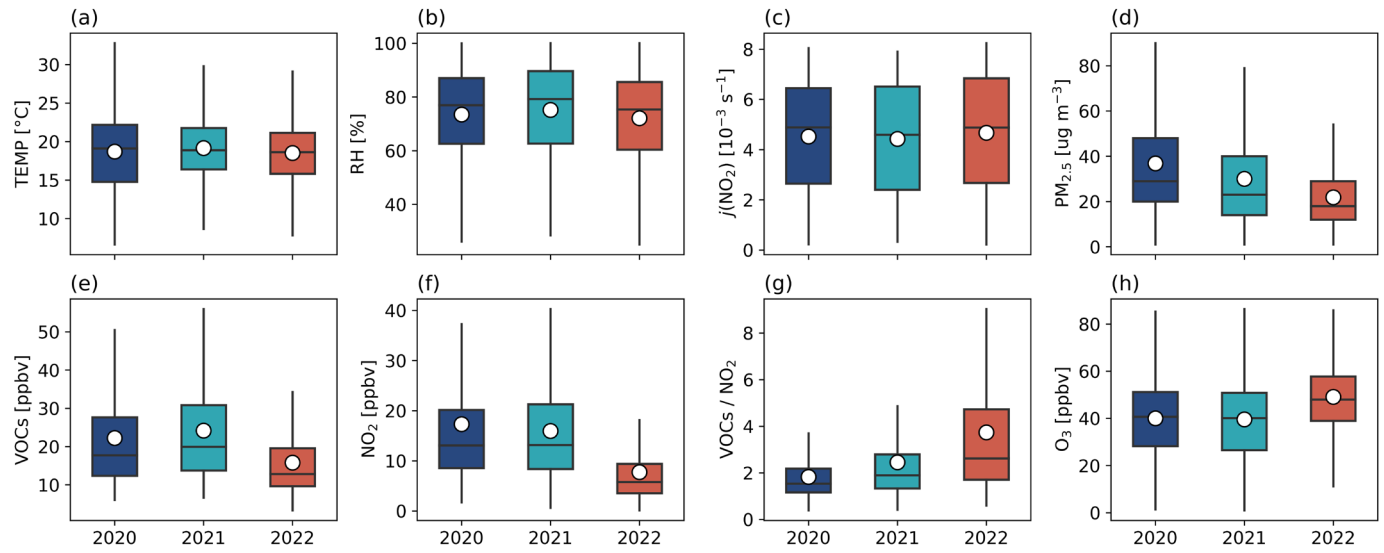
111 (Darby, 2005; Suris et al., 2022). The procedure for k-means clustering is as follows: (i) randomly initialize k clusters and then  
112 calculate the cluster centroid or mean, (ii) assign each data point to the nearest cluster using an appropriate distance measure, (iii)  
113 re-calculate the cluster centroids based on the current cluster members, (iv) repeat steps ii and iii until there is no further change.  
114 Additionally, the stacking model was applied to address missing values in DOAS observations caused by uncontrollable factors,  
115 ensuring the continuity and variation characteristics of the data. This step was deemed necessary for two main reasons. Firstly,  
116 the clustering analysis of O<sub>3</sub> diurnal variation demands a continuous time series without any missing values. Secondly, compared  
117 to the conventional method of handling missing data in the input of the OBM model through simple linear interpolation, the  
118 stacking model preserves the diurnal variation characteristics of the data, ensuring the correct constraints on the OBM model.  
119 The stacked model is an ensemble machine learning algorithm that consists of two levels, with two or more base models at level  
120 0 and one meta-model at level 1. The meta-model is trained using predictions made by the base models on out-of-sample data. In  
121 other words, data that was not used to train the base models is fed into them to make predictions. These predictions, along with  
122 the corresponding expected outputs, form the input and output pairs of the training dataset used to fit the meta-model. The  
123 stacking model has been previously described in detail and demonstrated good performance in Zhu et al. (2022), and the  
124 architecture of the stacking model can also be found in Figure S1. In this study, the models for O<sub>3</sub>, NO<sub>2</sub>, SO<sub>2</sub>, HONO, and  
125 HCHO demonstrated good performance, as shown in Figure S2-S6 of the Supplement.

## 126 3 Results and Discussion

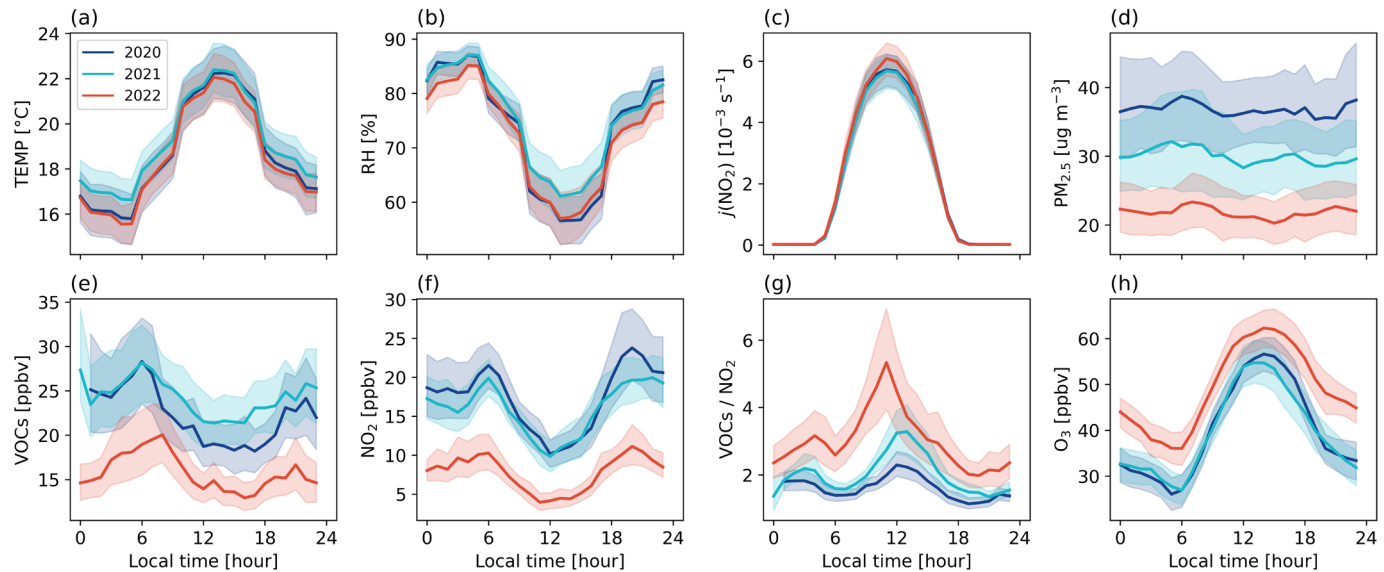
### 127 3.1 Year-on-year changes on air quality

128 Figure 1 compares the average levels of the meteorological parameters and air pollutants during the period from April to May of  
129 2020 to 2022, while Figure 2 compares the diurnal variations. In terms of meteorological parameters, the temperature and  
130 relative humidity, and  $j(\text{NO}_2)$  during the static management period in 2022 were almost unchanged compared to the same period  
131 in 2020 and 2021. The average temperature difference in 2022 was 6.5°C, which was similar to that of 2020 and slightly higher  
132 than that of 2021, while the average relative humidity at noon in 2022 was also comparable to that of 2020 and was 5% lower  
133 than that of 2021. Furthermore, we also ruled out the contribution of transport from the surrounding areas to the increase in  
134 ozone concentration in Shanghai during the 2022 static management period (see Figures S7-S10). The abrupt reduction of  
135 emissions across the entire industry led to a significant decrease in primary pollutant concentrations. The average concentrations  
136 of PM<sub>2.5</sub> in April and May from 2020 to 2022 were  $36.8 \pm 24.1$ ,  $30.0 \pm 23.1$ , and  $21.8 \pm 14.0 \text{ ug m}^{-3}$ , respectively, showing a  
137 decreasing trend over the years. And the diurnal variation profile in Figure 2d shows that PM<sub>2.5</sub> levels decreased proportionally  
138 throughout the entire 24-hour period, without any particularly prominent periods of decrease. The VOCs and NO<sub>2</sub> declined by 29%  
139 and 55% respectively compared to 2020, and by 35% and 51% respectively compared to 2021. Due to the significant decrease in  
140 NO<sub>2</sub> concentration compared to VOCs, the average ratio of VOCs/NO<sub>2</sub> has increased from 1.6 in 2020 to 3.0 in 2022. However,  
141 the precursor reduction at different magnitudes has led to an increase of approximately 23% in the average level of ozone. The  
142 photochemical production of ozone is controlled by the non-linear chemistry of the precursors VOCs and NO<sub>x</sub> (NO<sub>2</sub>+NO). The  
143 literatures have shown that Shanghai in the spring largely operates under VOCs-limited regime (Li et al., 2021a; Xue et al.,  
144 2022). Therefore, the reduction in VOCs during the static management period may not be enough to counteract the titration  
145 effect of NO<sub>x</sub>, and may even alter the ozone formation regime in Shanghai. From the perspective of diurnal variation (see Figure  
146 2), the period with a significant difference in the magnitude of the decrease between VOCs and NO<sub>2</sub> occurred during the strong  
147 photochemical process in the morning until noon. Therefore, the VOCs/NO<sub>2</sub> ratio during the static management period was  
148 significantly higher in the morning compared to the same period in 2020 and 2021. The weakening of the titration of nitrogen

149 oxides on ozone during nighttime led to significantly higher nighttime average levels during the static management period  
 150 compared to 2020 and 2021. Due to the higher  $O_3$  baseline concentration and higher VOCs/NO<sub>2</sub> ratio, there was a significant  
 151 increase in overall ozone levels.



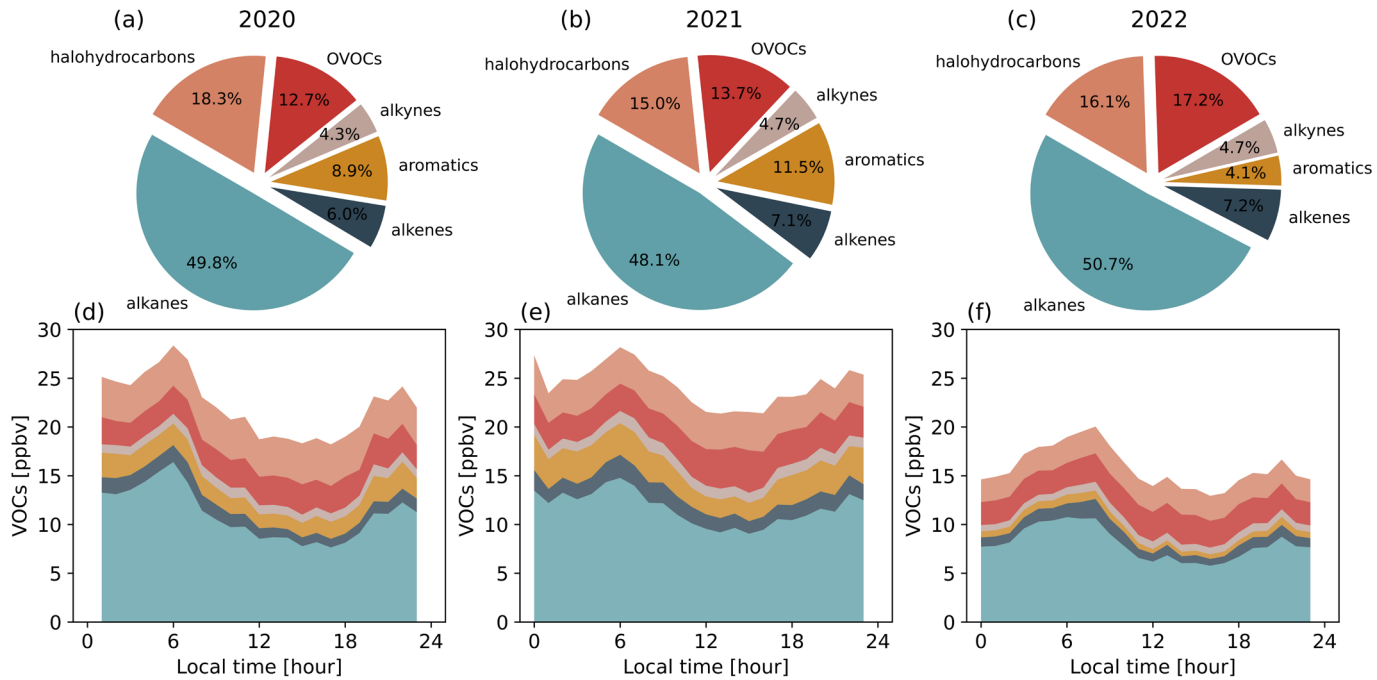
152  
 153 **Figure 1.** Comparison of meteorological parameters (TEMP, RH,  $j(NO_2)$ ) and air pollutants (PM<sub>2.5</sub>, VOCs, NO<sub>2</sub>, VOCs/NO<sub>2</sub>, O<sub>3</sub>)  
 154 during the periods from April to May of 2020, 2021, and 2022. The top and bottom of the vertical line for each box correspond to the  
 155 95th and 5th percentiles, respectively. The dots represent the averages, and the top, middle, and bottom lines of the box mark the 75th,  
 156 50th, and 25th percentiles, respectively.



157  
 158 **Figure 2.** The mean diurnal profiles of meteorological parameters and air pollutants during the periods from April to May of 2020,  
 159 2021, and 2022. Colored areas denote 95% confidence intervals.

160 As VOCs are crucial precursors for ozone formation, we conducted a comparison of each VOCs component during the 2022  
 161 static management period with those of the same period in 2020 and 2021, as shown in Figure 3. We classified the 103 VOCs  
 162 into six categories based on functional groups, including alkanes, alkenes, alkynes, aromatics, oxygenated VOCs (OVOCs), and  
 163 halohydrocarbons. The detailed classification is available in the Table S2. The results revealed that aromatics experienced the  
 164 most significant year-over-year reduction in absolute terms. The chemical raw materials and chemical products manufacturing  
 165 industry, which is the main source of aromatics (Liu et al., 2019), accounts for 10% of the total industrial output value, and this  
 166 industry experienced a 32% year-on-year decrease in total output value during the static management period

167 (https://tjj.sh.gov.cn/sjfb/index.html). In contrast, OVOCs remained relatively stable, primarily because they are sourced from  
 168 biogenic (Liu et al., 2019), and thus, were less impacted by lockdown measures relative to other VOCs. From the perspective of  
 169 ozone formation potential (OFP), in the years 2020 and 2021, the primary contributors were aromatics, followed by alkenes,  
 170 while in 2022, the primary contributors shifted to alkenes, with OVOCs coming in second (see Text S4 and Figure S11).  
 171 The reduction in the imbalance of VOCs has altered the average proportion of each component. Specifically, the proportion of  
 172 aromatics decreased from 8.9% and 11.5% to 4.1%, while the proportion of OVOCs increased from 12.7% and 13.7% to 17.2%.  
 173 The photolysis of OVOCs is a major source of the important radicals ROx ( $\text{OH}+\text{HO}_2+\text{RO}_2$ ) in the photochemical cycle, with a  
 174 daily average contribution rate of over 30% (Xue et al., 2016). In the radical chemistry section, the photolysis of OVOCs, as well  
 175 as the reactions of  $\text{O}_3$  and  $\text{NO}_3$  with VOCs, have been quantified for their contributions to the radicals. Additionally, the role of  
 176 VOCs in the propagation of radicals has been quantified.. The mean diurnal profiles of the VOCs indicated that the daily average  
 177 concentration range in 2020, 2021, and 2022 was between 18-28 ppbv, 21-28 ppbv, and 13-20 ppbv, respectively.  
 178 In 2022, the peak time of VOCs was observed at 08:00, which exhibited a delay compared to the peak times observed in 2020  
 179 and 2021 at 06:00, resembling the previously reported “weekend effect” on VOCs that the peak time of VOCs is delayed on  
 180 weekends in comparison to weekdays (Cai et al., 2010). In Figure S12 of Supplement, we observe that the peak of VOCs diurnal  
 181 profile in June 2023, after the lifting of restrictions, returned to 06:00. This finding indicates that the reduced human activities  
 182 during the 2022 period, similar to weekends, led to a decline in anthropogenic VOC emissions in the morning.



183  
 184 **Figure 3. The proportions (a, b, c) and the mean diurnal profiles (d, e, f) of different VOCs components during the periods from April**  
 185 **to May of 2020, 2021, and 2022.**

186

### 187 **3.2 Clustering of $\text{O}_3$ diurnal profiles**

188 The k-means algorithm clustered the ozone diurnal profiles over the three years into four types, as shown in Figure 4a. We define  
 189 the minimum concentration in the ozone diurnal profile as the background concentration, and the difference between the midday  
 190 peak and the morning trough represents the net ozone production. These four types of profiles can be described as follows:  
 191 Cluster 1 with low background concentration (22.4 ppbv) and low net production (14.8 ppbv); Cluster 2 with low background

concentration (16.9 ppbv) and high net production (45.9 ppbv); Cluster 3 with high background concentration (40.6 ppbv) and low net production (17.5 ppbv); and Cluster 4 with high background concentration (33.3 ppbv) and high net production (50.9 ppbv). The background concentration of ozone is mainly determined by the nighttime loss of ozone and the titration of nitrogen oxides in the morning, while the net production depends on the intensity of the photochemical reactions. In Figure 4b, the four ozone profiles occurred for 13, 24, 20, and 4 days in 2020, comparable occupation of 19, 21, 17, and 4 days in 2021, respectively. During the static management period of 2022, when the nitrogen oxide titration effect weakened, the number of days on which Cluster 3 and Cluster 4 appeared increased to 34 and 16, respectively. The average ozone levels for the four types were comparable across 2020, 2021, and 2022, ranging from 27-30 ppbv for Cluster 1, 38-40 ppbv for Cluster 2, 46-49 ppbv for Cluster 3, and 54-61 ppbv for Cluster 4 (Figure 4c). As depicted in Figure 4d, assuming that the proportions of the four types in 2022 are the same as those in 2020 and 2021, the average ozone levels in 2022 would decrease by 14.5% and 17.3%, respectively, remaining comparable to the levels in 2020 and 2021. Alternatively, if the proportions of the four types in 2020 and 2021 were the same as those in 2022, the average ozone levels in 2020 and 2021 would increase by 15.4% and 20.2%, respectively, which would be very close to the levels in 2022. Purely statistical analysis indicated that the significant high and stable level of ozone in 2022 was due to a higher proportion of Cluster 3 and Cluster 4, which had higher ozone concentrations during the static management period.

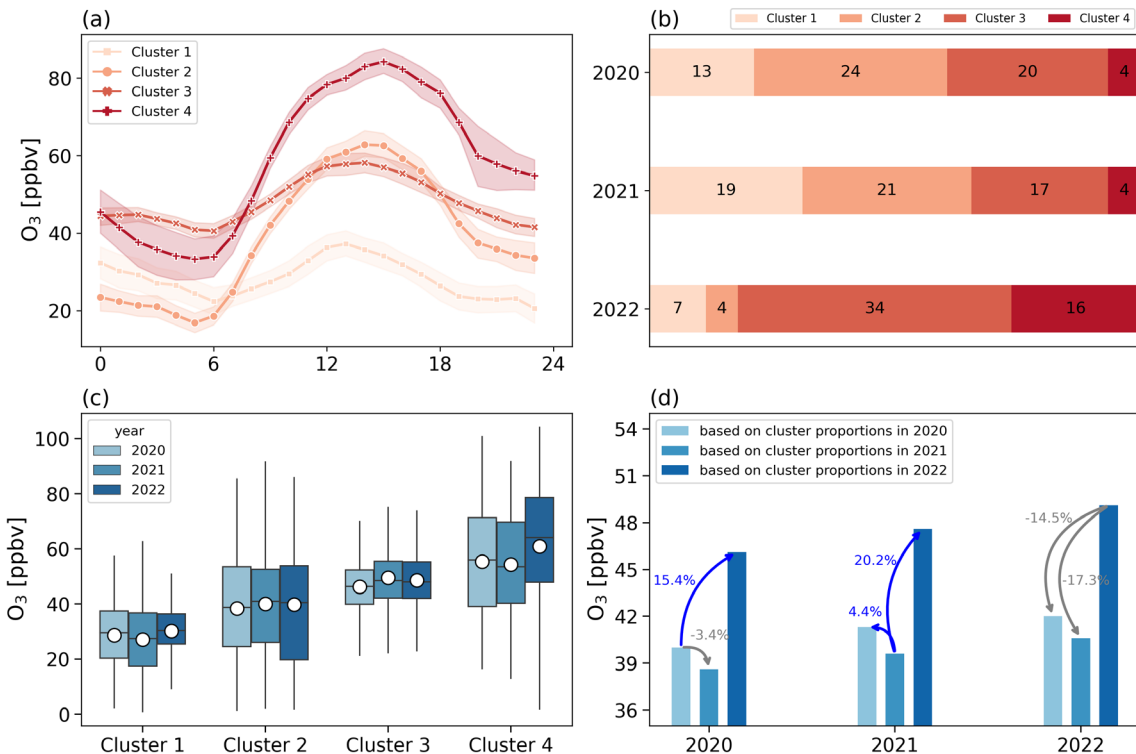
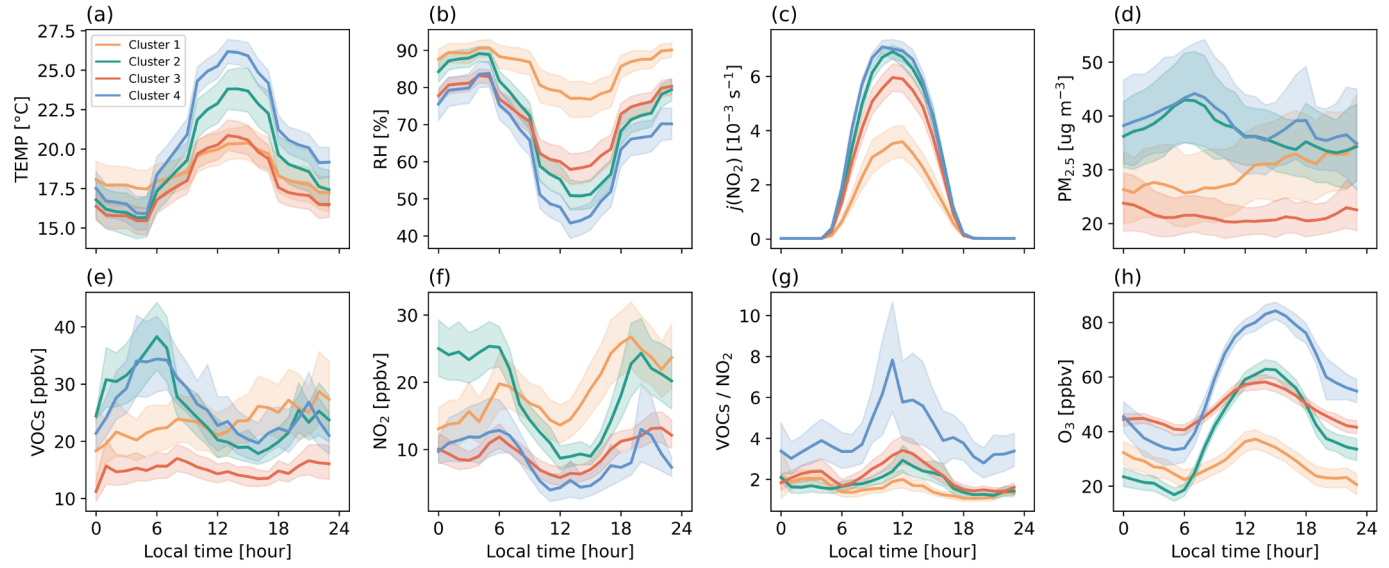


Figure 4. (a) Comparison of the mean diurnal profiles of the four types of O<sub>3</sub> after clustering. Colored areas denote 95% confidence intervals; (b) The proportions of the four clusters in 2020, 2021 and 2022. (c) Comparison of the O<sub>3</sub> levels of the four clusters in 2020, 2021 and 2022. The top and bottom of the vertical line for each box correspond to the 95th and 5th percentiles, respectively. The dots represent the averages, and the top, middle, and bottom lines of the box mark the 75th, 50th, and 25th percentiles, respectively; (d) Comparison of the average ozone concentrations in 2020, 2021 and 2022 for different ratios of the four clusters.

Different types of ozone profiles are formed under different meteorological conditions and pollution environments with distinctive diurnal variations. As shown in Figure 5, the meteorological conditions during the periods of Cluster 2 and Cluster 4, with high net ozone production, were characterized by high temperature, low relative humidity, and high radiation, compared to those during Cluster 1 and Cluster 3 periods. This is consistent with the well-known favorable condition promoting ozone production. The valley values of ozone profiles are closely related to the titration of nitrogen oxides, as shown in Figures 5f and

5h, where the valley values of ozone are inversely related to the peak values of  $\text{NO}_2$  during the morning rush hour. Indeed, it is these meteorological conditions and titration that result in the formation of the corresponding four clusters of ozone profiles. During periods of Cluster 2 and Cluster 4, a large amount of VOCs accumulated before sunrise and were rapidly consumed after sunrise. Similarly, the precursor  $\text{NO}_2$  was also rapidly consumed after sunrise, with the difference that the  $\text{NO}_2$  level during Cluster 4 was lower than that of Cluster 2. The diurnal profiles of  $\text{PM}_{2.5}$  under four clusters exhibit similar patterns to those of VOCs, with Cluster 2 and Cluster 4 exhibiting a distinct morning peak. The VOCs/ $\text{NO}_2$  ratio in Cluster 4 was significantly higher than that in other clusters, which may explain the substantial net ozone production despite the relatively high ozone background levels. The differences among the clusters are also reflected in the photochemical processes. In the following sections, we investigated the reasons for the increase in ozone levels during the static management period from the perspective of atmospheric oxidizing capacity and free radical chemistry.



228  
229 **Figure 5. The mean diurnal profiles of meteorological parameters and air pollutants for four clusters over three years. Colored areas**  
230 **denote 95% confidence intervals.**

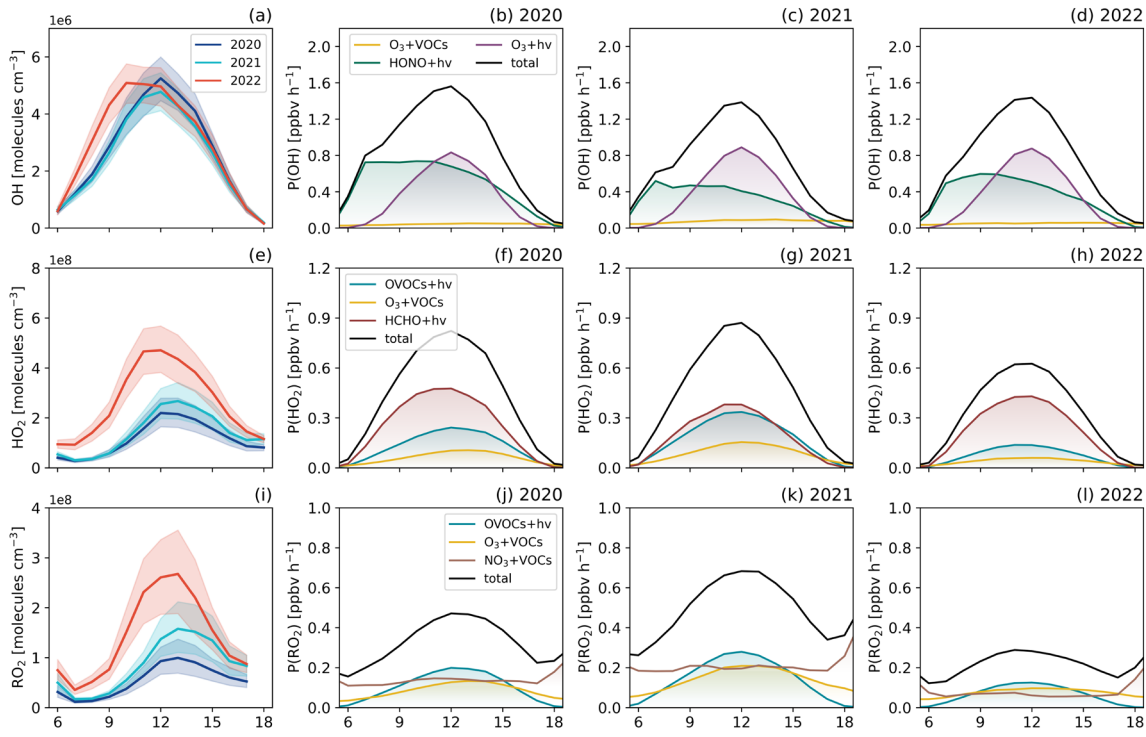
### 231 3.3 Radical chemistry

232 Figures 6a, 6e and 6i show the mean diurnal profiles of simulated  $\text{OH}$ ,  $\text{HO}_2$  and  $\text{RO}_2$  radical concentrations for the years 2020,  
233 2021, and 2022. These radicals exhibit clear diurnal variations, with peaks occurring at midday. The mean diurnal profiles  
234 display that the average peak concentrations of  $\text{OH}$  were  $5.2 \times 10^6$ ,  $4.8 \times 10^6$ , and  $5.1 \times 10^6$  molecules  $\text{cm}^{-3}$ , those of  $\text{HO}_2$  were  
235  $2.2 \times 10^8$ ,  $2.7 \times 10^8$ , and  $4.7 \times 10^8$  molecules  $\text{cm}^{-3}$ , and those of  $\text{RO}_2$  were  $0.9 \times 10^8$ ,  $1.6 \times 10^8$  and  $2.6 \times 10^8$  molecules  $\text{cm}^{-3}$  in  
236 2020, 2021 and 2022, respectively. The differences in radicals concentration levels were mainly reflected in the  $\text{HO}_2$  and  $\text{RO}_2$   
237 radicals. The average peak values of the  $\text{HO}_2$  and  $\text{RO}_2$  radicals in 2022 were about 1 to 3 times higher than those in the same  
238 periods of 2020 and 2021. Reviewing previous observational results, peak concentrations of  $\text{OH}$  and  $\text{HO}_2$  were observed at  
239 various locations and times (see Table S3):  $(4\text{-}17) \times 10^6$  molecules  $\text{cm}^{-3}$  and  $(2\text{-}24) \times 10^8$  molecules  $\text{cm}^{-3}$  at a suburban site in  
240 Yufa from Aug 18-31, 2006 (Lu et al., 2013);  $(5\text{-}15) \times 10^6$  molecules  $\text{cm}^{-3}$  and  $(3\text{-}14) \times 10^8$  molecules  $\text{cm}^{-3}$  at a rural site in  
241 Wangdu from June 8 to July 8, 2014 (Tan et al., 2017);  $4.5 \times 10^6$  molecules  $\text{cm}^{-3}$  and  $3 \times 10^8$  molecules  $\text{cm}^{-3}$  at a suburban in  
242 Heshan from October 22 to November 5, 2014 (Tan et al., 2019);  $(2\text{-}9) \times 10^6$  molecules  $\text{cm}^{-3}$  and  $(2\text{-}14) \times 10^8$  molecules  $\text{cm}^{-3}$  at  
243 a urban sites in Shenzhen from Oct 5-28, 2018 (Yang et al., 2022);  $(8\text{-}24) \times 10^6$  molecules  $\text{cm}^{-3}$  and  $(4\text{-}28) \times 10^8$  molecules  $\text{cm}^{-3}$   
244 at a suburban site in Taizhou from May 23 to June 18, 2018 (Ma et al., 2022); and  $(10\text{-}20) \times 10^6$  molecules  $\text{cm}^{-3}$  and  $(6\text{-}18) \times 10^8$   
245 molecules  $\text{cm}^{-3}$  at a suburban site in Chengdu from Aug 10-25, 2019 (Yang et al., 2021). The simulated concentrations of  $\text{OH}$

246 and HO<sub>2</sub> in this study were comparable to the observed levels during autumn in Shenzhen, which is also an urban site, however,  
247 were generally lower than those observed at non-urban sites. This difference can be attributed to the site types, but more  
248 importantly, to the fact that most observations were conducted during periods of stronger radiation. For RO<sub>2</sub>, the average  
249 maximum concentration was simulated to be  $4.5 \times 10^8$  molecules cm<sup>-3</sup> at urban site of Beijing in August 2007 (Liu et al., 2012).  
250 At coastal site of Xiamen, the simulated average daily peak reached  $4.7 \times 10^8$  molecules cm<sup>-3</sup> in September 2019, while at the  
251 coastal site of Ningde, the simulated value was  $0.9 \times 10^8$  molecules cm<sup>-3</sup> in spring 2019 (Liu et al., 2022). Overall, our RO<sub>x</sub>  
252 concentrations fell within the range of observations and simulated results in other regions of China. During the static  
253 management period in 2022, the levels of RO<sub>x</sub> were significantly higher compared to the same period in 2020 and 2021,  
254 indicating an enhanced atmospheric oxidation capacity in Shanghai in 2022.

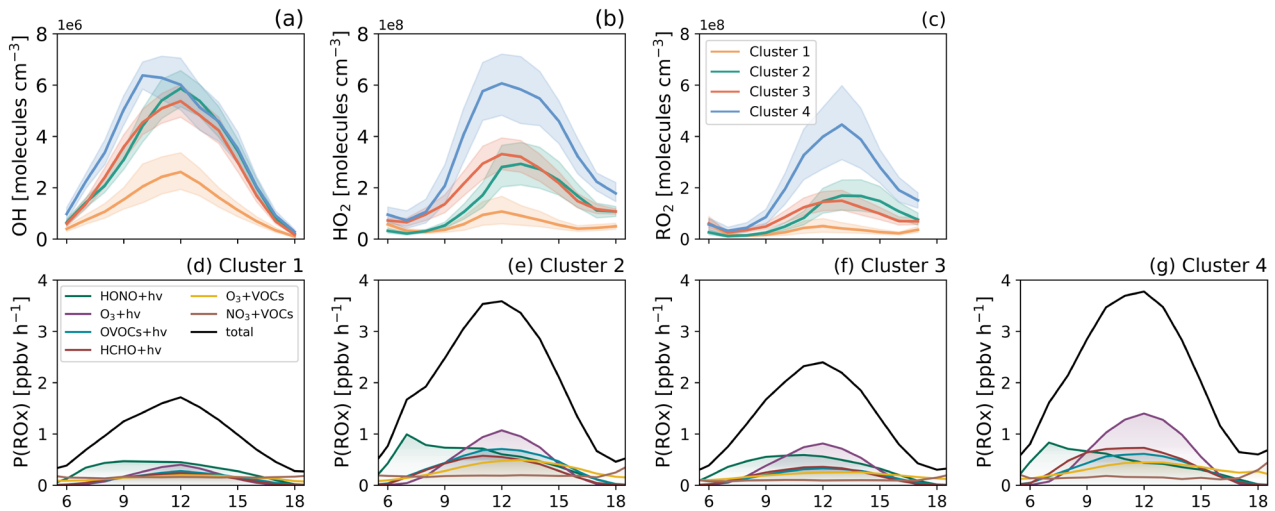
255 Figures 6b-6d, Figures 6f-6h, and Figures 6j-6l illustrate the mean diurnal variation of primary OH, HO<sub>2</sub>, and RO<sub>2</sub> sources for  
256 the years of 2020, 2021, and 2022. For OH, HONO photolysis peaked at around 07:00 and remained high until around 12:00,  
257 with peak values reaching approximately 0.72 ppbv h<sup>-1</sup>, 0.52 ppbv h<sup>-1</sup>, and 0.60 ppbv h<sup>-1</sup> in 2020, 2021, and 2022, respectively.  
258 Meanwhile, ozone photolysis peaked at noon, with peak values reaching around 0.83 ppbv h<sup>-1</sup>, 0.89 ppbv h<sup>-1</sup>, and 0.88 ppbv h<sup>-1</sup>,  
259 respectively. In addition, the ozonolysis of unsaturated VOCs was another source of OH radical, with an average production rate  
260 of less than 0.10 ppbv h<sup>-1</sup>, while other sources such as the photolysis of H<sub>2</sub>O<sub>2</sub>, HNO<sub>3</sub>, and OVOCs were generally negligible.  
261 Overall, HONO photolysis for the daytime accounted for 57%, 43%, and 48% of the total OH primary production rates in 2020,  
262 2021, and 2022, respectively, with O<sub>3</sub> photolysis accounting for 39%, 48%, and 46% in the corresponding years. For HO<sub>2</sub> radical,  
263 the most important source was HCHO photolysis, with average production rates during daytime of 0.28 ppbv h<sup>-1</sup>, 0.21 ppbv h<sup>-1</sup>,  
264 and 0.25 ppbv h<sup>-1</sup> in the corresponding years, respectively. The secondary source was OVOCs photolysis, which produce HO<sub>2</sub> at  
265 the average rate of 0.14 ppbv h<sup>-1</sup>, 0.20 ppbv h<sup>-1</sup>, and 0.08 ppbv h<sup>-1</sup>, respectively. Another source to consider was reactions of O<sub>3</sub>  
266 and unsaturated VOCs, which had an average rate of around 0.07 ppbv h<sup>-1</sup> for three years. For RO<sub>2</sub> radical, the daytime average  
267 peak of primary production rates contributed by OVOCs photolysis from 2020 to 2022 were 0.12 ppbv h<sup>-1</sup>, 0.16 ppbv h<sup>-1</sup>, and  
268 0.07 ppbv h<sup>-1</sup>, respectively. The reactions of O<sub>3</sub> and NO<sub>3</sub> with VOCs were also important primary sources of RO<sub>2</sub> radical. The primary  
269 production rate of RO<sub>2</sub> in 2022 was lower compared to the years 2020 and 2021. This can be attributed to the fact that the  
270 primary sources of RO<sub>2</sub> are the reactions involved VOCs, which significantly decreased during the static management period and  
271 further led to the decreased sources of RO<sub>2</sub>.

272 Overall, the total primary production rates of RO<sub>x</sub> in 2022 was 2.34 ppbv h<sup>-1</sup>, which is lower than 2.94 ppbv h<sup>-1</sup> and 2.85 ppbv h<sup>-1</sup>  
273 in 2021, as shown in Figure S13 of the Supplement. . These values are higher than the simulated value of 1.56 ppbv h<sup>-1</sup> in  
274 November 2019 in downtown Shanghai (Zhang et al., 2022a), but close to the value of 2.55 ppbv h<sup>-1</sup> during the ozone episode in  
275 the suburban of Shanghai in 2018 (Zhang et al., 2021). During these three years, reactions involving VOCs (excluding HCHO)  
276 accounted for 18.3%, 28.1%, and 26.5%, respectively, which is correlated with the observed VOCs abundances. In 2020 and  
277 2022, HONO photolysis accounted for 30.7% and 28.4% of the total primary production rates, respectively, with O<sub>3</sub> photolysis  
278 following at 20.9% and 27.2%. In 2021, the dominant contribution was from O<sub>3</sub> photolysis, reaching 21.4%, followed by HONO  
279 photolysis at 19.6%. Radical chemistry exhibits heterogeneity across different cities, with HONO photolysis being a primary  
280 source in New York (Ren et al., 2003), Paris (Michoud et al., 2012), Wangdu (Tan et al., 2017), and Taizhou (Ma et al., 2022).  
281 OVOC photolysis dominated in Mexico City (Sheehy et al., 2010), Hong Kong (Xue et al., 2016), and Beijing (Liu et al., 2012).  
282 Milan relied on HCHO photolysis as a major source (Alicke et al., 2002), while ozone photolysis was prominent in Nashville  
283 (Martinez et al., 2003).



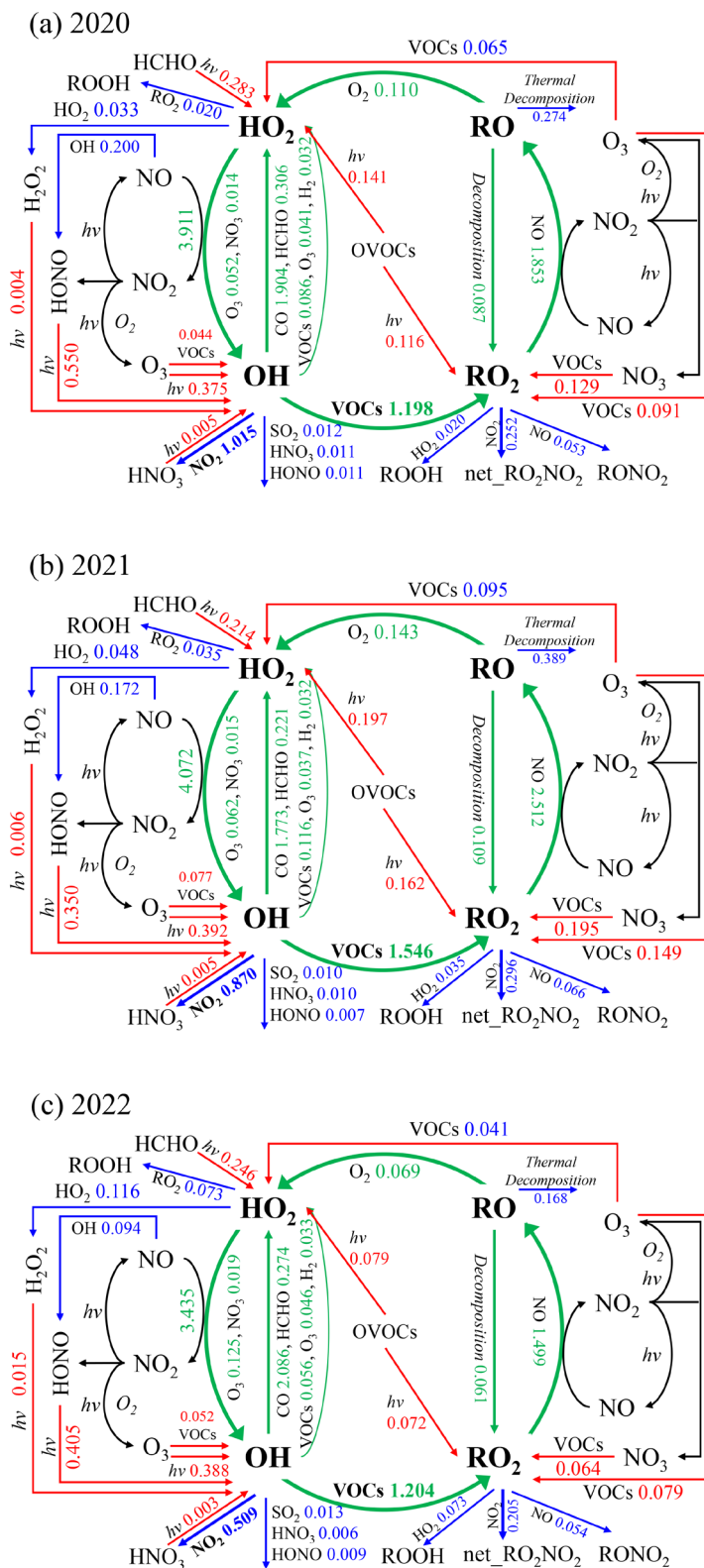
286  
 287 **Figure 6. The mean diurnal profiles of simulated OH (a), HO<sub>2</sub> (e), and RO<sub>2</sub> (i) concentrations in 2020, 2021, and 2022. Colored areas**  
 288 **denote 95% confidence intervals; The mean diurnal profiles of primary sources of OH radical (b-d), HO<sub>2</sub> radical (f-h), and RO<sub>2</sub>**  
 289 **radical (j-l) from model calculations in 2020, 2021 and 2022.**

290 We also investigated the radical chemistry under different ozone profile clusters (Figure 7). The average peak of OH in Cluster 1,  
 291 Cluster 2, Cluster 3, and Cluster 4 were  $2.6 \times 10^6$  molecules  $\text{cm}^{-3}$ ,  $5.9 \times 10^6$  molecules  $\text{cm}^{-3}$ ,  $5.4 \times 10^6$  molecules  $\text{cm}^{-3}$ , and  $6.4 \times$   
 292  $10^6$  molecules  $\text{cm}^{-3}$ , those of HO<sub>2</sub> were  $1.1 \times 10^8$  molecules  $\text{cm}^{-3}$ ,  $2.9 \times 10^8$  molecules  $\text{cm}^{-3}$ ,  $3.3 \times 10^8$  molecules  $\text{cm}^{-3}$ , and  $6.1 \times$   
 293  $10^8$  molecules  $\text{cm}^{-3}$ , and those of RO<sub>2</sub> were  $0.5 \times 10^8$  molecules  $\text{cm}^{-3}$ ,  $1.7 \times 10^8$  molecules  $\text{cm}^{-3}$ ,  $1.5 \times 10^8$  molecules  $\text{cm}^{-3}$ , and  
 294  $4.5 \times 10^8$  molecules  $\text{cm}^{-3}$ , respectively. Clearly, Cluster 4 had the highest levels of OH, HO<sub>2</sub>, and RO<sub>2</sub> radicals among all clusters,  
 295 with HO<sub>2</sub> and RO<sub>2</sub> radicals being particularly prominent. The average peak of P(RO<sub>x</sub>) for Clusters 1 to 4 were 1.71 ppbv h<sup>-1</sup>,  
 296 3.58 ppbv h<sup>-1</sup>, 2.39 ppbv h<sup>-1</sup>, and 3.77 ppbv h<sup>-1</sup>, respectively. Cluster 2 and Cluster 4, characterized by significant net ozone  
 297 production, exhibit distinct features in radical chemistry. The daily average of P(RO<sub>x</sub>) was 2.28 ppbv h<sup>-1</sup> in Cluster 2 and 2.37  
 298 ppbv h<sup>-1</sup> in Cluster 4, which is higher than the values of 1.08 ppbv h<sup>-1</sup> in Cluster 1 and 1.44 ppbv h<sup>-1</sup> in Cluster 3. In addition,  
 299 HONO photolysis during the morning rush hour was particularly prominent in Cluster 2 and Cluster 4, with peak values reaching  
 300 0.99 ppbv h<sup>-1</sup> and 0.83 ppbv h<sup>-1</sup>, respectively. In Cluster 2, HONO photolysis was the dominant source with a daily average of  
 301 0.56 ppbv h<sup>-1</sup>, accounting for 25% of the total, and ozone photolysis followed with 0.47 ppbv h<sup>-1</sup>, accounting for 21%. On the  
 302 other hand, in Cluster 4, ozone photolysis took the lead with 0.65 ppbv h<sup>-1</sup>, representing 27% of the total, and HONO photolysis  
 303 came next with 0.47 ppbv h<sup>-1</sup>, accounting for 20%. Additionally, OVOCs photolysis (including HCHO) in Cluster 2 and Cluster  
 304 4 showed a significant increase compared to Cluster 1 and Cluster 3. The correlation analysis between the each primary source of  
 305 radicals and the net ozone production reveals a significant correlation (see Figure S15), which shows that a large amount of net  
 306 ozone production implies the presence of active photochemical processes. Cluster 4 is characterized by higher concentrations of  
 307 HO<sub>2</sub> and RO<sub>2</sub> radicals and a higher primary source of radicals. Cluster 3 has moderate levels of radical concentrations and  
 308 primary sources of radicals, but it features a high ozone background value. The increase in the number of days associated with  
 309 these two clusters in 2022 has contributed to the elevated ozone levels.



310  
 311 **Figure 7. The mean diurnal profiles of simulated OH (a), HO<sub>2</sub> (b), and RO<sub>2</sub> (c) concentrations for Cluster 1, Cluster 2, Cluster 3, and**  
 312 **Cluster 4. Colored areas denote 95% confidence intervals; The mean diurnal profiles of primary sources of ROx radical (d-g) from**  
 313 **model calculations for Cluster 1, Cluster 2, Cluster 3, and Cluster 4.**

314 In tropospheric chemistry, radical initiation, which involves the breakdown of closed-shell species to generate new radicals,  
 315 plays a crucial role in initiating the formation of secondary pollutants. However, in highly polluted atmospheric environments,  
 316 radical cycling becomes the dominant process, with the amplification of new radicals in the ROx cycle playing a crucial role.  
 317 Volkamer et al. (2010) quantified the production of new radicals and found that approximately 20% of radical production is  
 318 attributed to the breakdown of closed-shell species, while 80% is derived from radical cycling. Therefore, in addition to  
 319 understanding the sources of radicals, it is essential to comprehend the impacts of radical cycling and recycling processes on  
 320 ozone formation. Figure 8 demonstrated the daytime average of ROx radicals budgets during the periods from April to May of  
 321 2020, 2021, and 2022. Taking the simulation of 2022 as an example, OH oxidation of CO and VOCs produces HO<sub>2</sub> and RO<sub>2</sub>  
 322 with daytime average rates of 2.09 ppbv h<sup>-1</sup> (1.90 ppbv h<sup>-1</sup> in 2020 and 1.77 ppbv h<sup>-1</sup> in 2021) and 1.20 ppbv h<sup>-1</sup> (1.20 ppbv h<sup>-1</sup> in  
 323 2020 and 1.55 ppbv h<sup>-1</sup> in 2021), respectively. The reactions of RO<sub>2</sub>+NO and HO<sub>2</sub>+NO further lead to the strong production of  
 324 RO with a rate of 1.50 ppbv h<sup>-1</sup> (1.85 ppbv h<sup>-1</sup> in 2020 and 2.51 ppbv h<sup>-1</sup> in 2021) and OH with a rate of 3.44 ppbv h<sup>-1</sup> (3.91 ppbv  
 325 h<sup>-1</sup> in 2020 and 4.07 ppbv h<sup>-1</sup> in 2021), while generating O<sub>3</sub> as a by-product. Clearly, these recycling processes dominate the  
 326 overall production of ROx radicals compared to the primary sources. The OH-HO<sub>2</sub> cycle is an important process in ozone  
 327 formation. According to the statistics in Table S3, no evidence was found to suggest that the cycle in 2022 was more efficient  
 328 than in 2020 and 2021. In terms of termination processes, the loss of ROx radicals was primarily dominated by their reactions  
 329 with NOx. Specifically, the reactions of OH+NO<sub>2</sub> and RO<sub>2</sub>+NO<sub>2</sub> accounted for approximately 0.51 ppbv h<sup>-1</sup> (1.01 ppbv h<sup>-1</sup> in  
 330 2020 and 0.87 ppbv h<sup>-1</sup> in 2021) and 0.21 ppbv h<sup>-1</sup> (0.25 ppbv h<sup>-1</sup> in 2020 and 0.30 ppbv h<sup>-1</sup> in 2021) of the ROx radical loss on  
 331 daytime average, respectively. This is in line with the understanding that reactions involving NOx typically play a dominant role  
 332 in the removal of radicals in high NOx environments (Zhang et al., 2021; Xue et al., 2016; Volkamer et al., 2010; Tan et al.,  
 333 2019; Liu et al., 2012). To sum up, the changes resulting from the approximately 55% reduction in NO<sub>2</sub> and 30% reduction in  
 334 VOCs due to static management are reflected in both the radical propagation and termination processes. The ratio of OH radical  
 335 propagation (OH+VOCs) to termination (OH+NO<sub>2</sub>) reached 2.37, which is higher than 1.18 in 2020 and 1.78 in 2021. It can be  
 336 inferred the different proportions of NO<sub>2</sub> and VOCs reduction did not weaken the radical cycling. On the contrary, a higher  
 337 VOCs/NO<sub>2</sub> ratio promotes the radical recycling efficiency in the reaction chain of radicals.



342 **4 Conclusions**

343 The two-month city-wide static management was implemented in April and May 2022 in Shanghai aiming to control the spread  
344 of the Omicron variant, providing a valuable opportunity to study the causes of ozone pollution. The comprehensive observations  
345 during the static management and same period in 2020 and 2021 show that there was a decrease of 29%-35% in VOCs and 51%-  
346 55% in NO<sub>2</sub> concentrations, while the average ozone level increased by nearly 23%. By statistics, the ozone profiles were  
347 classified into four clusters: Cluster 1, characterized by low background concentration and low net production; Cluster 2,  
348 characterized by low background concentration and high net production; Cluster 3, characterized by high background  
349 concentration and low net production; and Cluster 4, characterized by high background concentration and high net production.  
350 The average O<sub>3</sub> concentration relationship among these clusters is Cluster 4 > Cluster 3 > Cluster 2 > Cluster 1. The significant  
351 increase in the proportion of Cluster 4 and Cluster 3 during the period of static management led to an overall increase in average  
352 ozone levels. Secondly, from the perspective of radical chemistry, we explored the changes in photochemical processes due to  
353 the reduction in precursor species. The OBM model simulated the levels of radicals and their processes of initiation, propagation,  
354 and termination. The average peak concentrations of OH, HO<sub>2</sub>, and RO<sub>2</sub> in 2022 were  $5.1 \times 10^6$ ,  $4.7 \times 10^8$ , and  $2.6 \times 10^8$   
355 molecules cm<sup>-3</sup>, respectively, which were higher than those in the same period in 2020 and 2021. HONO photolysis was the main  
356 contributor to the primary source of ROx, accounting for about 30% of the total. However, in terms of the overall production of  
357 ROx radicals, the radical recycling process remained dominant. The different proportions of NO<sub>2</sub> and VOCs reduction during  
358 static management led to an increased OH radical propagation (OH+VOCs) to termination (OH+NO<sub>2</sub>) ratio, reaching 2.37,  
359 higher than 1.18 in 2020 and 1.78 in 2021. This enhanced ratio indicates a strengthened radical cycling as a result of a higher  
360 VOCs/NO<sub>2</sub> ratio.

361 The important lesson from the static management “large-scale field experiment” is that Shanghai operates in a VOCs-limited  
362 regime. When the reduction in VOCs is not able to catch up with or exceed the reduction in nitrogen oxides, it is not sufficient to  
363 curb the formation of secondary pollutants. In terms of ozone control strategies, it is necessary to strengthen the regulation and  
364 control of VOCs.

365 **Data Availability**

366 The observed and predicted hourly time series data in the study are presented in Figure S16-S18, and Code and data used for our  
367 analyses are available at <https://data.mendeley.com/datasets/3kmhg7r2df/1> (Zhu, 2023).

368 **Competing interests**

369 The contact author has declared that none of the authors has any competing interests.

370 **Author contributions**

371 Jian Zhu: Conceptualization, Methodology, Software, Validation, Investigation, Writing original draft, Visualization. Shanshan  
372 Wang: Conceptualization, Methodology, Supervision, Funding acquisition. Chuanqi Gu, Zhiwen Jiang, Sanbao Zhang, Ruibin  
373 Xue, and Yuhao Yan: Methodology, Validation, Investigation. Bin Zhou: Conceptualization, Methodology, Supervision,  
374 Funding acquisition.

375 **Acknowledgments**

376 This work was supported by National Natural Science Foundation of China (22176037, 42075097, 22376030, 42375089,  
377 21976031) and National Key Research and Development Program of China (2022YFC3700101).

380 Agarwal, A., Kaushik, A., Kumar, S., and Mishra, R. K.: Comparative study on air quality status in Indian and Chinese cities  
 381 before and during the COVID-19 lockdown period, *Air Quality, Atmosphere & Health*, 13, 1167-1178,  
 382 <https://doi.org/10.1007/s11869-020-00881-z>, 2020.

383 Alicke, B., Platt, U., and Stutz, J.: Impact of nitrous acid photolysis on the total hydroxyl radical budget during the Limitation of  
 384 Oxidant Production/Pianura Padana Produzione di Ozono study in Milan, *Journal of Geophysical Research: Atmospheres*, 107,  
 385 LOP 9-1-LOP 9-17, <https://doi.org/10.1029/2000JD000075>, 2002.

386 Bao, R. and Zhang, A.: Does lockdown reduce air pollution? Evidence from 44 cities in northern China, *Science of the Total  
 387 Environment*, 731, 139052, <https://doi.org/10.1016/j.scitotenv.2020.139052>, 2020.

388 Cai, C., Geng, F., Tie, X., Yu, Q., and An, J.: Characteristics and source apportionment of VOCs measured in Shanghai, China,  
 389 *Atmospheric Environment*, 44, 5005-5014, <https://doi.org/10.1016/j.atmosenv.2010.07.059>, 2010.

390 Chu, B., Zhang, S., Liu, J., Ma, Q., and He, H.: Significant concurrent decrease in PM<sub>2.5</sub> and NO<sub>2</sub> concentrations in China during  
 391 COVID-19 epidemic, *Journal of Environmental Sciences*, 99, 346-353, <https://doi.org/10.1016/j.jes.2020.06.031>, 2021.

392 Darby, L. S.: Cluster analysis of surface winds in Houston, Texas, and the impact of wind patterns on ozone, *Journal of Applied  
 393 Meteorology and Climatology*, 44, 1788-1806, <https://doi.org/10.1175/JAM2320.1>, 2005.

394 Ding, J., van der A, R. J., Eskes, H., Mijling, B., Stavrakou, T., Van Geffen, J., and Veefkind, J.: NO<sub>x</sub> emissions reduction and  
 395 rebound in China due to the COVID - 19 crisis, *Geophysical Research Letters*, 47, e2020GL089912,  
 396 <https://doi.org/10.1029/2020GL089912>, 2020.

397 Feng, S., Jiang, F., Wang, H., Wang, H., Ju, W., Shen, Y., Zheng, Y., Wu, Z., and Ding, A.: NO<sub>x</sub> emission changes over China  
 398 during the COVID - 19 epidemic inferred from surface NO<sub>2</sub> observations, *Geophysical Research Letters*, 47, e2020GL090080,  
 399 <https://doi.org/10.1029/2020GL090080>, 2020.

400 Gu, C., Wang, S., Zhu, J., Wu, S., Duan, Y., Gao, S., and Zhou, B.: Investigation on the urban ambient isoprene and its oxidation  
 401 processes, *Atmospheric Environment*, 270, 118870, <https://doi.org/10.1016/j.atmosenv.2021.118870>, 2022.

402 Guo, Y., Wang, S., Zhu, J., Zhang, R., Gao, S., Saiz-Lopez, A., and Zhou, B.: Atmospheric formaldehyde, glyoxal and their  
 403 relations to ozone pollution under low-and high-NO<sub>x</sub> regimes in summertime Shanghai, China, *Atmospheric Research*, 258,  
 404 105635, <https://doi.org/10.1016/j.atmosres.2021.105635>, 2021.

405 Hua, J., Zhang, Y., de Foy, B., Shang, J., Schauer, J. J., Mei, X., Sulaymon, I. D., and Han, T.: Quantitative estimation of  
 406 meteorological impacts and the COVID-19 lockdown reductions on NO<sub>2</sub> and PM<sub>2.5</sub> over the Beijing area using Generalized  
 407 Additive Models (GAM), *Journal of Environmental Management*, 291, 112676, <https://doi.org/10.1016/j.jenvman.2021.112676>,  
 408 2021.

409 Huang, X., Ding, A., Gao, J., Zheng, B., Zhou, D., Qi, X., Tang, R., Wang, J., Ren, C., and Nie, W.: Enhanced secondary  
 410 pollution offset reduction of primary emissions during COVID-19 lockdown in China, *National Science Review*, 8, nwaa137,  
 411 <https://doi.org/10.1093/nsr/nwaa137>, 2021.

412 Jenkin, M., Saunders, S., Wagner, V., and Pilling, M.: Protocol for the development of the Master Chemical Mechanism, MCM  
 413 v3 (Part B): tropospheric degradation of aromatic volatile organic compounds, *Atmospheric Chemistry and Physics*, 3, 181-193,  
 414 <https://doi.org/10.5194/acp-3-181-2003>, 2003.

415 Li, D., Wang, S., Xue, R., Zhu, J., Zhang, S., Sun, Z., and Zhou, B.: OMI-observed HCHO in Shanghai, China, during 2010–  
 416 2019 and ozone sensitivity inferred by an improved HCHO/NO<sub>2</sub> ratio, *Atmospheric Chemistry and Physics*, 21, 15447-15460,  
 417 <https://doi.org/10.5194/acp-21-15447-2021>, 2021a.

418 Li, R., Zhao, Y., Fu, H., Chen, J., Peng, M., and Wang, C.: Substantial changes in gaseous pollutants and chemical compositions  
 419 in fine particles in the North China Plain during the COVID-19 lockdown period: anthropogenic vs. meteorological influences,  
 420 *Atmospheric Chemistry and Physics*, 21, 8677-8692, <https://doi.org/10.5194/acp-21-8677-2021>, 2021b.

421 Liu, C. and Shi, K.: A review on methodology in O<sub>3</sub>-NO<sub>x</sub>-VOC sensitivity study, *Environmental Pollution*, 291, 118249,  
 422 <https://doi.org/10.1016/j.envpol.2021.118249>, 2021.

423 Liu, T., Hong, Y., Li, M., Xu, L., Chen, J., Bian, Y., Yang, C., Dan, Y., Zhang, Y., and Xue, L.: Atmospheric oxidation capacity  
 424 and ozone pollution mechanism in a coastal city of southeastern China: analysis of a typical photochemical episode by an  
 425 observation-based model, *Atmospheric Chemistry and Physics*, 22, 2173-2190, <https://doi.org/10.5194/acp-22-2173-2022>, 2022.

426 Liu, T., Wang, X., Hu, J., Wang, Q., An, J., Gong, K., Sun, J., Li, L., Qin, M., and Li, J.: Driving forces of changes in air quality  
 427 during the COVID-19 lockdown period in the Yangtze River Delta Region, China, *Environmental Science & Technology Letters*,  
 428 7, 779-786, <https://doi.org/10.1021/acs.estlett.0c00511>, 2020.

429 Liu, Y., Wang, H., Jing, S., Gao, Y., Peng, Y., Lou, S., Cheng, T., Tao, S., Li, L., and Li, Y.: Characteristics and sources of  
 430 volatile organic compounds (VOCs) in Shanghai during summer: Implications of regional transport, *Atmospheric Environment*,  
 431 215, 116902, <https://doi.org/10.1016/j.atmosenv.2019.116902>, 2019.

432 Liu, Z., Wang, Y., Gu, D., Zhao, C., Huey, L. G., Stickel, R., Liao, J., Shao, M., Zhu, T., and Zeng, L.: Summertime  
 433 photochemistry during CAREBeijing-2007: ROx budgets and O<sub>3</sub> formation, *Atmospheric Chemistry and Physics*, 12, 7737-7752,  
 434 <https://doi.org/10.5194/acp-12-7737-2012>, 2012.

435 Lu, K., Hofzumahaus, A., Holland, F., Bohn, B., Brauers, T., Fuchs, H., Hu, M., Häseler, R., Kita, K., and Kondo, Y.: Missing  
 436 OH source in a suburban environment near Beijing: observed and modelled OH and HO<sub>2</sub> concentrations in summer 2006,  
 437 *Atmospheric Chemistry and Physics*, 13, 1057-1080, <https://doi.org/10.5194/acp-13-1057-2013>, 2013.

438 Ma, X., Tan, Z., Lu, K., Yang, X., Chen, X., Wang, H., Chen, S., Fang, X., Li, S., and Li, X.: OH and HO<sub>2</sub> radical chemistry at a  
439 suburban site during the EXPLORE-YRD campaign in 2018, *Atmospheric Chemistry and Physics*, 22, 7005-7028,  
440 <https://doi.org/10.5194/acp-22-7005-2022>, 2022.

441 Martinez, M., Harder, H., Kovacs, T., Simpas, J., Bassis, J., Lesher, R., Brune, W., Frost, G., Williams, E., and Stroud, C.: OH  
442 and HO<sub>2</sub> concentrations, sources, and loss rates during the Southern Oxidants Study in Nashville, Tennessee, summer 1999,  
443 *Journal of Geophysical Research: Atmospheres*, 108, <https://doi.org/10.1029/2003JD003551>, 2003.

444 Michoud, V., Kukui, A., Camredon, M., Colomb, A., Borbon, A., Miet, K., Aumont, B., Beekmann, M., Durand-Jolibois, R., and  
445 Perrier, S.: Radical budget analysis in a suburban European site during the MEGAPOLI summer field campaign, *Atmospheric  
446 Chemistry and Physics*, 12, 11951-11974, <https://doi.org/10.5194/acp-12-11951-2012>, 2012.

447 Rana, R. H., Keramat, S. A., and Gow, J.: A systematic literature review of the impact of COVID-19 lockdowns on air quality in  
448 China, *Aerosol and Air Quality Research*, 21, 200614, <https://doi.org/10.4209/aaqr.200614>, 2021.

449 Ren, X., Harder, H., Martinez, M., Lesher, R. L., Olinger, A., Shirley, T., Adams, J., Simpas, J. B., and Brune, W. H.: HO<sub>x</sub>  
450 concentrations and OH reactivity observations in New York City during PMTACS-NY2001, *Atmospheric Environment*, 37,  
451 3627-3637, [https://doi.org/10.1016/S1352-2310\(03\)00460-6](https://doi.org/10.1016/S1352-2310(03)00460-6), 2003.

452 Santiago, J.-L., Martilli, A., and Martin, F.: On dry deposition modelling of atmospheric pollutants on vegetation at the  
453 microscale: Application to the impact of street vegetation on air quality, *Boundary-layer meteorology*, 162, 451-474,  
454 <https://doi.org/10.1007/s10546-016-0210-5>, 2017.

455 Saunders, S. M., Jenkin, M. E., Derwent, R., and Pilling, M.: Protocol for the development of the Master Chemical Mechanism,  
456 MCM v3 (Part A): tropospheric degradation of non-aromatic volatile organic compounds, *Atmospheric Chemistry and Physics*, 3,  
457 161-180, <https://doi.org/10.5194/acp-3-161-2003>, 2003.

458 Sheehy, P., Volkamer, R., Molina, L. T., and Molina, M. J.: Oxidative capacity of the Mexico City atmosphere-Part 2: A RO<sub>x</sub>  
459 radical cycling perspective, *Atmospheric Chemistry and Physics*, 10, 6993-7008, <https://doi.org/10.5194/acp-10-6993-2010>,  
460 2010.

461 Shi, X. and Brasseur, G. P.: The response in air quality to the reduction of Chinese economic activities during the COVID - 19  
462 outbreak, *Geophysical Research Letters*, 47, e2020GL088070, <https://doi.org/10.1029/2020GL088070>, 2020.

463 Sillman, S.: The relation between ozone, NO<sub>x</sub> and hydrocarbons in urban and polluted rural environments, *Atmospheric  
464 Environment*, 33, 1821-1845, [https://doi.org/10.1016/S1352-2310\(98\)00345-8](https://doi.org/10.1016/S1352-2310(98)00345-8), 1999.

465 Sommariva, R., Cox, S., Martin, C., Borońska, K., Young, J., Jimack, P. K., Pilling, M. J., Matthaios, V. N., Nelson, B. S., and  
466 Newland, M. J.: AtChem (version 1), an open-source box model for the Master Chemical Mechanism, *Geoscientific Model  
467 Development*, 13, 169-183, <https://doi.org/10.5194/gmd-13-169-2020>, 2020.

468 Suris, F. N. A., Bakar, M. A. A., Ariff, N. M., Mohd Nadzir, M. S., and Ibrahim, K.: Malaysia PM<sub>10</sub> air quality time series  
469 clustering based on dynamic time warping, *Atmosphere*, 13, 503, <https://doi.org/10.3390/atmos13040503>, 2022.

470 Tan, Y. and Wang, T.: What caused ozone pollution during the 2022 Shanghai lockdown? Insights from ground and satellite  
471 observations, *Atmospheric Chemistry and Physics*, 22, 14455-14466, <https://doi.org/10.5194/acp-22-14455-2022>, 2022.

472 Tan, Z., Fuchs, H., Lu, K., Hofzumahaus, A., Bohn, B., Broch, S., Dong, H., Gomm, S., Häseler, R., and He, L.: Radical  
473 chemistry at a rural site (Wangdu) in the North China Plain: observation and model calculations of OH, HO<sub>2</sub> and RO<sub>2</sub> radicals,  
474 *Atmospheric Chemistry and Physics*, 17, 663-690, <https://doi.org/10.5194/acp-17-663-2017>, 2017.

475 Tan, Z., Lu, K., Hofzumahaus, A., Fuchs, H., Bohn, B., Holland, F., Liu, Y., Rohrer, F., Shao, M., and Sun, K.: Experimental  
476 budgets of OH, HO<sub>2</sub>, and RO<sub>2</sub> radicals and implications for ozone formation in the Pearl River Delta in China 2014, *Atmospheric  
477 chemistry and physics*, 19, 7129-7150, <https://doi.org/10.5194/acp-19-7129-2019>, 2019.

478 Tian, J., Wang, Q., Zhang, Y., Yan, M., Liu, H., Zhang, N., Ran, W., and Cao, J.: Impacts of primary emissions and secondary  
479 aerosol formation on air pollution in an urban area of China during the COVID-19 lockdown, *Environment International*, 150,  
480 106426, <https://doi.org/10.1016/j.envint.2021.106426>, 2021.

481 Venter, Z. S., Aunan, K., Chowdhury, S., and Lelieveld, J.: COVID-19 lockdowns cause global air pollution declines,  
482 *Proceedings of the National Academy of Sciences*, 117, 18984-18990, <https://doi.org/10.1073/pnas.200685311>, 2020.

483 Volkamer, R., Sheehy, P., Molina, L. T., and Molina, M. J.: Oxidative capacity of the Mexico City atmosphere-Part 1: A radical  
484 source perspective, *Atmospheric Chemistry and Physics*, 10, 6969-6991, <https://doi.org/10.5194/acp-10-6969-2010>, 2010.

485 Wang, N., Xu, J., Pei, C., Tang, R., Zhou, D., Chen, Y., Li, M., Deng, X., Deng, T., and Huang, X.: Air quality during COVID-  
486 19 lockdown in the Yangtze River Delta and the Pearl River Delta: Two different responsive mechanisms to emission reductions  
487 in China, *Environmental Science & Technology*, 55, 5721-5730, <https://doi.org/10.1021/acs.est.0c08383>, 2021.

488 Wang, P., Chen, K., Zhu, S., Wang, P., and Zhang, H.: Severe air pollution events not avoided by reduced anthropogenic  
489 activities during COVID-19 outbreak, *Resources, Conservation and Recycling*, 158, 104814,  
490 <https://doi.org/10.1016/j.resconrec.2020.104814>, 2020.

491 Wang, T., Xue, L., Brimblecombe, P., Lam, Y. F., Li, L., and Zhang, L.: Ozone pollution in China: A review of concentrations,  
492 meteorological influences, chemical precursors, and effects, *Science of the Total Environment*, 575, 1582-1596,  
493 <https://doi.org/10.1016/j.scitotenv.2016.10.081>, 2017.

494 Xue, L., Gu, R., Wang, T., Wang, X., Saunders, S., Blake, D., Louie, P. K., Luk, C. W., Simpson, I., and Xu, Z.: Oxidative  
495 capacity and radical chemistry in the polluted atmosphere of Hong Kong and Pearl River Delta region: analysis of a severe  
496 photochemical smog episode, *Atmospheric Chemistry and Physics*, 16, 9891-9903, <https://doi.org/10.5194/acp-16-9891-2016>,  
497 2016.

498 Xue, R., Wang, S., Zhang, S., Zhan, J., Zhu, J., Gu, C., and Zhou, B.: Ozone Pollution of Megacity Shanghai during City-Wide  
499 Lockdown Assessed Using TROPOMI Observations of NO<sub>2</sub> and HCHO, *Remote Sensing*, 14, 6344,  
500 <https://doi.org/10.3390/rs14246344>, 2022.

501 Yang, X., Lu, K., Ma, X., Gao, Y., Tan, Z., Wang, H., Chen, X., Li, X., Huang, X., and He, L.: Radical chemistry in the Pearl  
502 River Delta: observations and modeling of OH and HO<sub>2</sub> radicals in Shenzhen in 2018, *Atmospheric Chemistry and Physics*, 22,  
503 12525-12542, <https://doi.org/10.5194/acp-22-12525-2022>, 2022.

504 Yang, X., Lu, K., Ma, X., Liu, Y., Wang, H., Hu, R., Li, X., Lou, S., Chen, S., and Dong, H.: Observations and modeling of OH  
505 and HO<sub>2</sub> radicals in Chengdu, China in summer 2019, *Science of The Total Environment*, 772, 144829,  
506 <https://doi.org/10.1016/j.scitotenv.2020.144829>, 2021.

507 Zhang, G., Hu, R., Xie, P., Lou, S., Wang, F., Wang, Y., Qin, M., Li, X., Liu, X., and Wang, Y.: Observation and simulation of  
508 HO<sub>x</sub> radicals in an urban area in Shanghai, China, *Science of The Total Environment*, 810, 152275,  
509 <https://doi.org/10.1016/j.scitotenv.2021.152275>, 2022a.

510 Zhang, H., Ho, T.-B., and Lin, M.-S.: An evolutionary K-means algorithm for clustering time series data, *Proceedings of 2004*  
511 *International Conference on Machine Learning and Cybernetics (IEEE Cat. No. 04EX826)*, 1282-1287,  
512 <https://doi.org/10.1109/ICMLC.2004.1382390>,

513 Zhang, K., Huang, L., Li, Q., Huo, J., Duan, Y., Wang, Y., Yaluk, E., Wang, Y., Fu, Q., and Li, L.: Explicit modeling of  
514 isoprene chemical processing in polluted air masses in suburban areas of the Yangtze River Delta region: radical cycling and  
515 formation of ozone and formaldehyde, *Atmospheric Chemistry and Physics*, 21, 5905-5917, <https://doi.org/10.5194/acp-21-5905-2021>, 2021.

516 Zhang, K., Liu, Z., Zhang, X., Li, Q., Jensen, A., Tan, W., Huang, L., Wang, Y., de Gouw, J., and Li, L.: Insights into the  
517 significant increase in ozone during COVID-19 in a typical urban city of China, *Atmospheric Chemistry and Physics*, 22, 4853-  
518 4866, <https://doi.org/10.5194/acp-22-4853-2022>, 2022b.

519 Zhu, J.: Why Did Ozone Concentrations Increase During Shanghai's Static Management? A Statistical and Radical Chemistry  
520 Perspective (V1), Mendeley Data [dataset], 10.17632/3kmhg7r2df.1, 2023.

521 Zhu, J., Wang, S., Zhang, S., Xue, R., Gu, C., and Zhou, B.: Changes of NO<sub>3</sub> Radical and its Nocturnal Chemistry in Shanghai  
522 from 2014 to 2021 Revealed by Long - term observation and a Stacking Model: Impact of China's Clean Air Action Plan,  
523 *Journal of Geophysical Research: Atmospheres*, e2022JD037438, <https://doi.org/10.1029/2022JD037438>, 2022.

524 Zhu, J., Wang, S., Wang, H., Jing, S., Lou, S., Saiz-Lopez, A., and Zhou, B.: Observationally constrained modeling of  
525 atmospheric oxidation capacity and photochemical reactivity in Shanghai, China, *Atmospheric Chemistry and Physics*, 20, 1217-  
526 1232, <https://doi.org/10.5194/acp-20-1217-2020>, 2020.

527

528